

September 12, 2018

# Long range rapidity correlations in soft interaction at high energies.

---

**E. Gotsman<sup>a\*</sup>, E. Levin<sup>a,b†</sup> and U. Maor<sup>a ‡</sup>**

*a) Department of Particle Physics, School of Physics and Astronomy, Raymond and Beverly Sackler Faculty of Exact Science, Tel Aviv University, Tel Aviv, 69978, Israel*

*b) Departamento de Física, Universidad Técnica Federico Santa María, Avda. España 1680 and Centro Científico-Tecnológico de Valparaíso, Casilla 110-V, Valparaíso, Chile*

**ABSTRACT:** In this paper we take the next step (following the successful description of inclusive hadron production) in describing the structure of the bias events without the aid of Monte Carlo codes. Two new results are presented : (i) a method for calculating the two particle correlation functions in the BFKL Pomeron calculus in zero transverse dimension; and (ii) an estimation of the values of these correlations in a model of soft interactions. Comparison with the multiplicity data at the LHC is given.

**KEYWORDS:** Soft Pomeron, BFKL Pomeron, Diffractive Cross Sections, Survival Probability.

*PACS: 13.85.-t, 13.85.Hd, 11.55.-m, 11.55.Bq*

---

\*Email: gotsman@post.tau.ac.il.

†Email: leving@post.tau.ac.il

‡Email: maor@post.tau.ac.il.

---

## Contents

<b>1. Introduction</b>	<b>1</b>
<b>2. Correlation function in the BFKL Pomeron Calculus in zero transverse dimensions</b>	<b>2</b>
2.1 General approach	2
2.2 Generating function approach	5
2.3 Amplitude in the MPSI approach: general formula	6
2.4 MPSI approximation: instructive examples	7
2.4.1 Glauber-Gribov formula	7
2.4.2 Summing 'fan' diagrams	8
2.4.3 Single inclusive production in MPSI approximation	9
2.5 The Correlation function in MPSI approximation	10
<b>3. Correlations in a model for soft interactions</b>	<b>11</b>
3.1 Estimates of the rapidity correlation function	12
3.2 Improvement of the model	13
3.3 Rapidity long range correlations in GLM model for soft interactions at high energy	15
3.3.1 The main ingredients of the GLM model	15
3.3.2 Formulae for the double inclusive cross section	16
3.3.3 Correlations in the GLM model	18
<b>4. Conclusions</b>	<b>19</b>

---

## 1. Introduction

The goal of this paper is twofold: to consider the two hadron long range rapidity correlations in the BFKL Pomeron Calculus in zero transverse dimensions; and to calculate these correlations in a model of soft interactions at high energy. The BFKL Pomeron Calculus in zero transverse dimension describes the interaction of the Pomerons through the triple Pomeron vertex ( $G_{3P}$ ) with a Pomeron intercept  $\Delta_P \equiv$

$\Delta > 0$  and a Pomeron slope  $\alpha'_{\mathcal{P}} = 0$ . The theory that includes all these ingredients can be formulated in a functional integral form [1]:

$$Z[\Phi, \Phi^+] = \int D\Phi D\Phi^+ e^S \quad \text{with} \quad S = S_0 + S_I + S_E, \quad (1.1)$$

where,  $S_0$  describes free Pomerons,  $S_I$  corresponds to their mutual interaction and  $S_E$  relates to the interaction with the external sources (target and projectile). Since  $\alpha'_{\mathcal{P}} = 0$ ,  $S_0$  has the form

$$S_0 = \int dY \Phi^+(Y) \left\{ -\frac{d}{dY} + \Delta \right\} \Phi(Y). \quad (1.2)$$

$S_I$  includes only triple Pomeron interactions and has the form

$$S_I = G_{3\mathcal{P}} \int dY \{ \Phi(Y) \Phi^+(Y) \Phi^+(Y) + h.c. \}. \quad (1.3)$$

For  $S_E$  we have local interactions both in rapidity and in impact parameter space,

$$S_E = - \int dY \sum_{i=1}^2 \{ \Phi(Y) g_i(b) + \Phi^+(Y) g_i(b) \}, \quad (1.4)$$

where,  $g_i(b)$  stands for the interaction vertex with the hadrons at fixed  $b$ .

At the moment this theory has two facets. First, it is a toy-model describing the interaction of the BFKL Pomerons in QCD. Many problems can be solved analytically in this simple model leading to a set of possible scenarios for the solution in BFKL Pomeron calculus [1–7]. Our first goal is to find an analytical solution for the correlation function in rapidity defined as

$$R(y_1, y_2) = \frac{\frac{1}{\sigma_{in}} \frac{d^2\sigma}{dy_1 dy_2}}{\frac{1}{\sigma_{in}} \frac{d\sigma}{dy_1} \frac{1}{\sigma_{in}} \frac{d\sigma}{dy_2}}, \quad (1.5)$$

where,  $\sigma_{in}$ ,  $d^2\sigma/dy_1 dy_2$  and  $d\sigma/dy$  are inelastic, double and single inclusive cross sections. We consider this problem as the most natural starting point to search for a solution for  $R(y_1, y_2)$ , in a more general and more difficult approach based on high density QCD.

On the other hand, recent experience in building models for high energy scattering [8–13] shows that a Pomeron with  $\alpha'_{\mathcal{P}} = 0$  can describe the experimental data including that at the LHC. It also appears in N=4 SYM [14–18] with a large coupling, which at the moment, is the only theory that allows one to treat the strong interaction on a theoretical basis. Therefore, our second goal is to evaluate the correlation function  $R(y_1, y_2)$  in our model for soft high energy interactions (see [8–10]).

## 2. Correlation function in the BFKL Pomeron Calculus in zero transverse dimensions

### 2.1 General approach

It is well known [19] that the most appropriate framework to discuss the inclusive processes has been developed by A.H. Mueller [20] (Mueller diagrams). In Fig. 1 we show the most general Mueller diagram

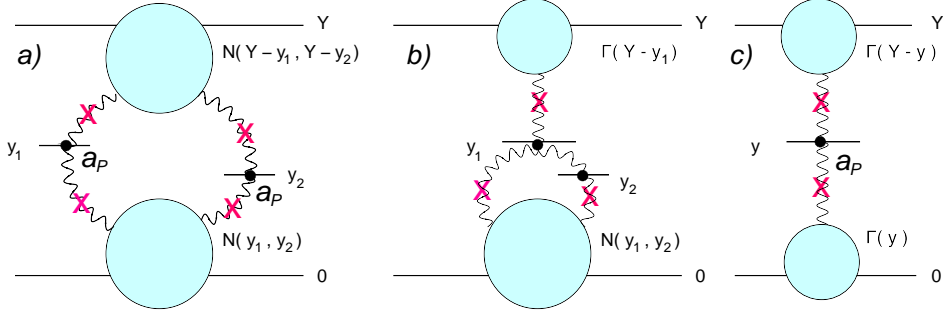


**Figure 1:** The Mueller diagram [20] for double (Fig. 1-a and b) and single (Fig. 1-c) inclusive cross section. The wavy lines denote Pomerons. The cross on a wavy line indicates that this line describes a cut Pomeron.

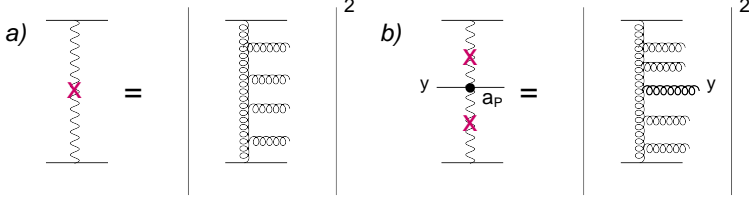


**Figure 2:** Shows the main ingredients of Fig. 1: the cut Pomeron that describes the process of multiparticle (multigluon) production (Fig. 2-a) and the single inclusive production from the cut Pomeron (Fig. 2-b).

for the double inclusive cross section (see also Fig. 2). From Fig. 1-a one can see that it is necessary to calculate the amplitudes of the cut Pomeron interaction with the hadrons, denoted by  $N(Y - y_1, Y - y_2)$  and  $N(y_1, y_2)$ . The fact that we can reduce the calculation of the double inclusive production to an evaluation of  $N(Y - y_1, Y - y_2)$  and  $N(y_1, y_2)$  stems from the AGK cutting rules [21] which state that the exchanges of the Pomerons from the top to the bottom of the Mueller diagram cancel each other leading to the general structure of Fig. 1-a. Recall that the AGK cutting rules are violated in QCD due to the emission diagrams from the triple Pomeron vertex (see Fig. 1-b) (see Ref. [22]). In our treatment we neglect such a violation since  $\Gamma(Y - y_1)$  turns out to be smaller at high energy than  $N(Y - y_1, Y - y_2)$ . Indeed, in the first approximation  $\Gamma(Y - y_1) \propto ge^{\Delta(Y - y_1)}$  while  $N(Y - y_1, Y - y_2) \propto \left(ge^{\Delta(Y - y_1)}\right)^2$  and  $\Gamma(Y - y_1) / N(Y - y_1, Y - y_2) \rightarrow 0$  at large values of  $Y - y_1$ . Analyzing the diagrams one can see that their contributions are proportional to two parameters which are large at high energy:

$$L(Y) = g(b) \frac{G_{3P}}{\Delta} e^{\Delta Y}; \quad \text{and} \quad T(Y) = \frac{G_{3P}^2}{\Delta^2} e^{\Delta Y}. \quad (2.1)$$

Note that  $\Delta$  in the dominator stems from the integration over internal rapidities of the triple Pomeron vertices. We consider the first three diagrams (see Fig. 3) for  $\Gamma(Y - y)$  (see Fig. 1) to illustrate how these two parameters appear in the calculations. For the diagrams of Fig. 3-a, Fig. 3-b and Fig. 3-c we have,

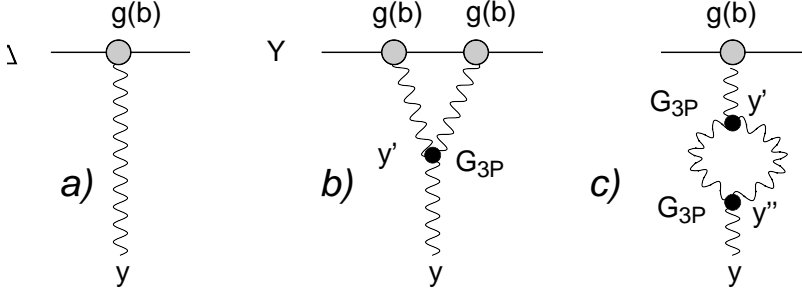


**Figure 3:** Low order diagrams for  $\Gamma(Y-y)$  (see Fig. 1). Wavy lines denote the Pomerons.

respectively,

$$A(\text{Pomeron}) = g(b) e^{\Delta(Y-y)}; \quad (2.2)$$

$$\begin{aligned} A(\text{'fan' diagram}) &= -g^2(b) G_{3P} \int_0^Y dy' e^{2\Delta(Y-y')} e^{\Delta y'} \\ &= -g(b) e^{\Delta(Y-y)} \left( L(Y-y) - g(b) \frac{G_{3P}}{\Delta} \right) \\ &\xrightarrow{Y-y \gg 1} -A(\text{Pomeron}) L(Y-y); \end{aligned} \quad (2.3)$$

$$\begin{aligned} A(\text{enhanced diagram}) &= -g^2(b) G_{3P}^2 \int_0^Y dy' \int_0^{y'} dy'' e^{\Delta(Y-y')} e^{2\Delta(y'-y'')} e^{\Delta y''} \\ &= -g(b) e^{\Delta(Y-y)} \left( T(Y-y) - g(b) \frac{G_{3P}^2}{\Delta^2} (1 + \Delta(Y-y)) \right) \\ &\xrightarrow{Y-y \gg 1} -A(\text{Pomeron}) T(Y-y); \end{aligned} \quad (2.4)$$

At high energy both  $L(Y) \gg 1$  and  $T(Y) \gg 1$  and we can neglect other contributions in each diagram.

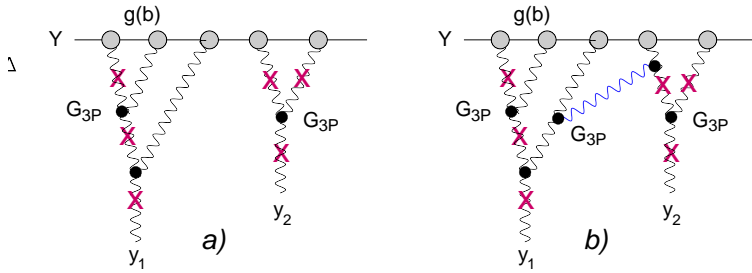


**Figure 4:** The main diagrams relating to  $L(Y-y_i)$  (see text), that contribute to the function  $N(Y-y_1, Y-y_2)$  (Fig. 4-a); and the first diagram with correction that is proportional to  $T(Y-y_i)$  (Fig. 4-b). Wavy lines denote the Pomerons. The cross on the wavy line indicates that this line describes the cut Pomeron.

In this kinematic region each Pomeron diagram is proportional to powers of  $L(Y)$  and  $T(Y)$ . Therefore, the first approximation is to sum the largest contributions at high energies in every Pomeron diagram. Such an approach to high energy scattering was proposed by Mueller, Patel, Salam and Iancu (MPSI approximation [23]). It turns out that the value of  $G_{3P}$  is rather small (see discussion below). Based on this fact we propose that the leading approximation shall be to sum all contributions proportional to  $L^n(Y-y)$  having in mind the following kinematic region:

$$L(Y-y) \geq 1; \quad T(Y-y) \ll 1; \quad g(b) \ll 1; \quad G_{3P} \ll 1. \quad (2.5)$$

For the scattering with nuclei  $g(b) \propto A^{1/3}$ , and in this region which covers all reasonable energies, the main contribution emanates from 'fan' diagrams (see Fig. 4 and Fig. 3- b for the first diagram of this kind). The expression for  $\Gamma(Y - y)$  is known [24, 25]:

$$\Gamma(Y - y) = \frac{2g e^{\Delta(Y-y)}}{1 + L(Y - y)}; \quad (2.6)$$

As we shall see below the factor 2 stems from the initial cut Pomeron. Below we shall obtain these expressions using a more general technique in which we find the sum of the diagrams in a more general kinematic region:

$$L(Y - y) \geq 1; \quad T(Y - y) \geq 1; \quad g(b) \ll 1; \quad G_{3P} \ll 1, \quad (2.7)$$

selecting contributions of the order of  $L^m(Y - y) T^{n-m}(Y - y)$ . i.e. we shall find the scattering amplitude in the kinematic region of Eq. (2.7) using MPSI approximation.

The most important diagrams for  $N(Y - y_1, Y - y_2)$  are shown in Fig. 3-a. One can see that the kinematic region of Eq. (2.5)  $N(Y - y_1, Y - y_2)$  is:

$$N(Y - y_1, Y - y_2) = \Gamma(Y - y_1) \Gamma(Y - y_2). \quad (2.8)$$

## 2.2 Generating function approach

We believe that the method of a generating function (functional) is the most appropriate method for summing Pomeron diagrams. In the MPSI approach, one can explicitly see the conservation of probability (unitarity constraints) in each step of the evolution in rapidity. This method was proposed by Mueller in Ref. [4] and has been developed in a number of publications(see Ref. [26] and references therein). In Ref. [27] it was generalized to account for the contribution to the inelastic processes by summing both cut and uncut Pomeron contributions. For completeness of the presentation, in this section we shall discuss the main features of this method, referring to Refs. [9, 10, 27] for essential details. Following Ref. [27], we introduce the generating function

$$Z(w, \bar{w}, v|Y) = \sum_{k=0} \sum_{l=0} \sum_{m=0} P(k, l, m|Y) w^k \bar{w}^l v^m, \quad (2.9)$$

where,  $P(k, l, m|Y)$  stands for the probability to find  $k$  uncut Pomerons in the amplitude,  $l$  uncut Pomerons in the conjugate amplitude and  $m$  cut Pomerons at some rapidity  $Y$ .  $w, \bar{w}$  and  $v$  are independent variables. Restricting ourselves by taking into account only a Pomeron splitting into two Pomerons, we can write the following simple evolution equation:

$$\frac{\partial Z}{\partial Y} = -\Delta \left\{ w(1-w) \frac{\partial Z}{\partial w} - \bar{w}(1-\bar{w}) \frac{\partial Z}{\partial \bar{w}} \right\} - \Delta \left\{ 2w\bar{w} - 2wv - 2\bar{w}v + v^2 + v \right\} \frac{\partial Z}{\partial v}. \quad (2.10)$$

Fig. 5 illustrates the two steps of evolution in rapidity for  $Z(w, \bar{w}, v; Y)$ . The general solution to Eq. (2.10) has the form

$$C_1 Z(w) + C_1 Z(\bar{w}) + C_2 Z(w + \bar{w} - v), \quad (2.11)$$

where,  $C_1$  and  $C_2$  are constants and  $Z(\xi)$  is the solution to the equation:

$$\frac{\partial Z}{\partial Y} = -\Delta\xi(1-\xi)\frac{\partial Z}{\partial\xi}. \quad (2.12)$$

The particular form of  $Z$  and the values of  $C_i$  are determined by the initial condition at  $Y = 0$ .

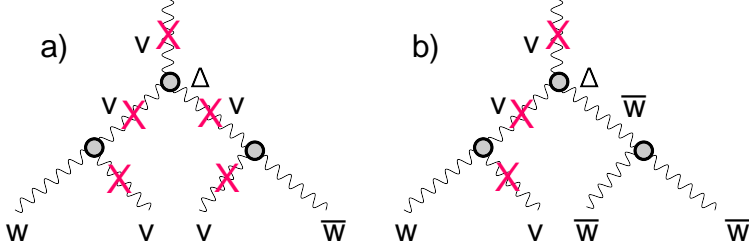


**Figure 5:** Two examples for two steps of evolution in rapidity for the generating function  $Z(w, \bar{w}, v; Y)$ . Wavy lines denote the Pomerons. The cross on the wavy line indicates that this line describes the cut Pomeron.

### 2.3 Amplitude in the MPSI approach: general formula

The general formula for the amplitude in the MPSI approach has the form (see Ref. [27])

$$N^{MPSI}(\gamma, \gamma_{in}|Y) = \left( \exp \left\{ -\gamma \frac{\partial}{\partial\gamma^{(1)}} \frac{\partial}{\partial\gamma^{(2)}} - \gamma \frac{\partial}{\partial\bar{\gamma}^{(1)}} \frac{\partial}{\partial\bar{\gamma}^{(2)}} + \gamma_{in} \frac{\partial}{\partial\gamma_{in}^{(1)}} \frac{\partial}{\partial\gamma_{in}^{(2)}} \right\} - 1 \right) Z(\gamma^{(1)}, \bar{\gamma}^{(1)}, \gamma_{in}^{(1)}|Y - Y') Z(\gamma^{(2)}, \bar{\gamma}^{(2)}, \gamma_{in}^{(2)}|Y') \Big|_{\gamma^{(i)}=\bar{\gamma}^{(i)}=\gamma_{in}^{(i)}=0}, \quad (2.13)$$

where,  $w = 1 - \gamma$ ,  $\bar{w} = 1 - \bar{\gamma}$  and  $v = 1 - \gamma_{in}$ .

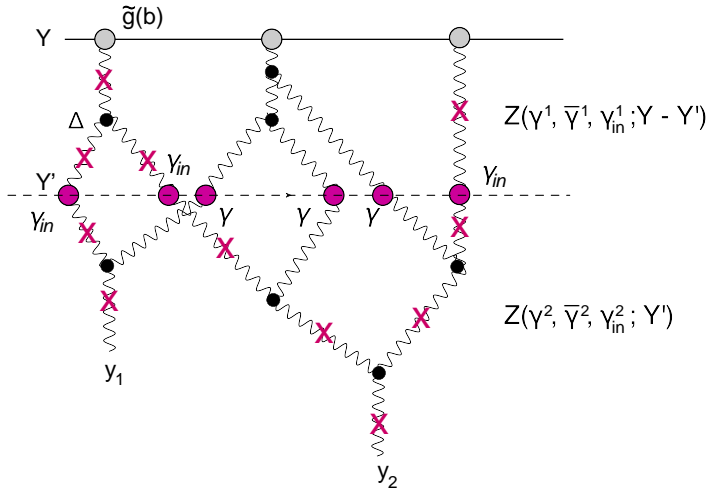


**Figure 6:** An example of diagrams that contribute to the function  $N(Y - y_1, Y - y_2)$  (see Fig. 1). Wavy lines denote the Pomerons. The cross on the wavy line indicates that this line describes a cut Pomeron.  $\gamma$  is the amplitude of the dipole-dipole interaction at low energies. The particular set of diagrams shown in this figure, corresponds to the MPSI approach [23].

Eq. (2.13) has a very simple meaning which is clear from Fig. 6. The derivatives of the generating functional  $Z(\gamma^{(1)}, \bar{\gamma}^{(1)}, \gamma_{in}^{(1)}|Y - Y')$  determine the probability to have cut and uncut Pomerons at  $Y = Y'$ , while the derivatives of  $Z(\gamma^{(2)}, \bar{\gamma}^{(2)}, \gamma_{in}^{(2)}|Y')$  lead to the probabilities of the creation of cut and uncut

Pomerons from two initial cut Pomerons at rapidity  $Y'$ . Two uncut Pomerons interact with the amplitude  $\gamma$  at rapidity  $Y'$  and with the amplitude  $\gamma_{in}$  in the case of cut Pomerons. The phases of the amplitude are given by related signs in Eq. (2.13): minus for  $\gamma$  and plus for  $\gamma_{in}$ . In addition, we assume that the low energy at which the wee partons from two Pomerons interact is large enough to assume that  $\gamma$  and  $\gamma_{in}$  are purely imaginary. We denote the imaginary part of the amplitude, by  $\gamma$ 's. It follows from the AGK cutting rules that

$$\gamma_{in} = 2\gamma. \quad (2.14)$$

According to Eq. (2.13), the contribution to the scattering amplitude of one Pomeron exchange is equal to \*

$$\tilde{g} e^{\Delta(Y-Y')} \gamma e^{\Delta Y'} \tilde{g}. \quad (2.15)$$

For the first 'fan' diagram, Eq. (2.13) leads to the following contribution:

$$\tilde{g} \int_{Y'}^Y dy' e^{\Delta(Y-y')} \Delta e^{2\Delta(y'-Y')} \gamma^2, e^{2\Delta(Y')} \tilde{g}^2, \quad (2.16)$$

while the first enhanced diagram can be written as

$$\tilde{g} \int_{Y'}^Y dy' e^{\Delta(Y-y')} \Delta e^{2\Delta(y'-Y')} \gamma^2 \int_0^{Y'} dy'' e^{2\Delta(Y'-y'')} \Delta e^{\Delta y''} \tilde{g}. \quad (2.17)$$

Comparing these expressions with the Pomeron diagrams (see Eq. (2.2), Eq. (2.3) and Eq. (2.4)), we have the correspondence between these two approaches,

$$\tilde{g} = g/\sqrt{\gamma}; \quad \gamma = \frac{G_{3P}^2}{\Delta^2}. \quad (2.18)$$

## 2.4 MPSI approximation: instructive examples

### 2.4.1 Glauber-Gribov formula

The pattern of calculation of Glauber-Gribov rescatterings due to Pomeron exchanges is shown in Fig. 7-a. The forms of the generating functions  $Z(\gamma^{(1)}, \bar{\gamma}^{(1)}, \gamma_{in}^{(1)} | Y - Y')$  and  $Z(\gamma^{(2)}, \bar{\gamma}^{(2)}, \gamma_{in}^{(2)} | Y')$  are simple,

$$Z(\gamma^{(1)}, \bar{\gamma}^{(1)}, \gamma_{in}^{(1)} | Y - Y') = e^{\tilde{g} e^{\Delta(Y-Y')} (w^{(1)} + \bar{w}^{(1)} - v^{(1)} - 1)} = e^{\tilde{g} e^{\Delta(Y-Y')} (\gamma^{(1)} + \bar{\gamma}^{(1)} - \gamma_{in}^{(1)})}; \quad (2.19)$$

$$Z(\gamma^{(2)}, \bar{\gamma}^{(2)}, \gamma_{in}^{(2)} | Y') = e^{\tilde{g} e^{\Delta(Y')} (w^{(2)} + \bar{w}^{(2)} - v^{(2)} - 3)} = e^{\tilde{g} e^{\Delta(Y')} (\gamma^{(2)} + \bar{\gamma}^{(2)} - \gamma_{in}^{(2)})}. \quad (2.20)$$

These generating functions describe the independent (without correlations) interaction of Pomerons with the target and the projectile. In the case of nuclei, Pomerons interact with different nucleons in the nucleus, and the correlations between nucleons in the wave function of the nucleus are neglected. Note that Eq. (2.13) with  $Z$ 's from Eq. (2.19) and Eq. (2.20) do not depend on the sign of  $v$  ( $\gamma_{in}$ ). However,

---

\*We suppress the notation of the impact parameter, which if needed can be easily be replaced.

we shall see below that the choice of the above equation is correct since it reproduces Eq. (2.6), which has been derived by summing the Pomeron diagrams.

Using Eq. (2.13), we can calculate the inelastic cross section requiring that at rapidity  $Y'$  we have at least one cut Pomeron (one  $\gamma_{in}$ ). The result is:

$$\sigma_{in} = 1 - e^{-\gamma_{in}\tilde{g}^2 e^{\Delta Y}} = 1 - e^{-2g^2 e^{\Delta Y}}. \quad (2.21)$$

which reproduces the well known expression for the inelastic cross section in the Glauber-Gribov approach.

We can also calculate the contribution which has no cut Pomeron at rapidity  $Y'$  (elastic cross sections). It has the form

$$\sigma_{el} = \left(1 - e^{-\gamma\tilde{g}^2 e^{\Delta Y}}\right) \left(1 - e^{-\bar{\gamma}\tilde{g}^2 e^{\Delta Y}}\right) = \left(1 - e^{-g^2 e^{\Delta Y}}\right)^2. \quad (2.22)$$

The total cross section is given by:

$$\sigma_{tot} = \sigma_{el} + \sigma_{in} = 2\left(1 - e^{-g^2 e^{\Delta Y}}\right). \quad (2.23)$$

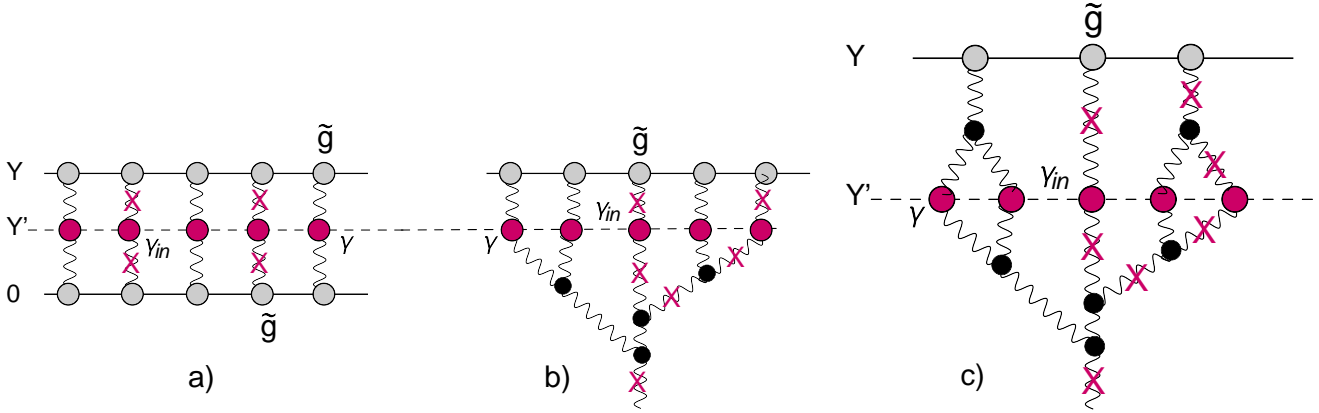


**Figure 7:** MPSI approximation: Glauber-Gribov rescattering (Fig. 7-a), summation of 'fan' diagrams (Fig. 7-b) and the diagrams for single inclusive cross section (Fig. 7-c) Wavy lines denote the Pomerons. The cross on the wavy line indicates that this line describes the cut Pomeron.  $\gamma$  is the amplitude of the dipole-dipole interaction at low energies.

#### 2.4.2 Summing 'fan' diagrams

As one can see from Fig. 7-b, the form of  $Z\left(\gamma^{(1)}, \bar{\gamma}^{(1)}, \gamma_{in}^{(1)} | Y - Y'\right)$  is the same as in the previous problem. It is given by Eq. (2.19). To obtain an expression for  $Z\left(\gamma^{(2)}, \bar{\gamma}^{(2)}, \gamma_{in}^{(2)} | Y'\right)$ , we need to find  $Z$ 's and  $C_i$  in Eq. (2.11) with the initial condition

$$Z\left(\gamma^{(2)}, \bar{\gamma}^{(2)}, \gamma_{in}^{(2)} | Y' = 0\right) = v. \quad (2.24)$$

The resulting solution is of the form (see more details in Ref. [27])

$$Z(w, \bar{w}, v; Y') = Z_{el}(w, \bar{w}; Y') + Z_{in}(w, \bar{w}, v; Y'); \quad (2.25)$$

$$Z_{el}(w, \bar{w}; Y') = \frac{w e^{-\Delta Y'}}{1 + w(e^{-\Delta Y'} - 1)} + \frac{\bar{w} e^{-\Delta Y'}}{1 + \bar{w}(e^{-\Delta Y'} - 1)} - \frac{(w + \bar{w})e^{-\Delta Y'}}{1 + (w + \bar{w})(e^{-\Delta Y'} - 1)}; \quad (2.26)$$

$$Z_{in}(w, \bar{w}, v; Y') = \frac{(w + \bar{w})e^{-\Delta Y'}}{1 + (w + \bar{w})(e^{-\Delta Y'} - 1)} - \frac{(w + \bar{w} - v)e^{-\Delta Y'}}{1 + (w + \bar{w} - v)(e^{-\Delta Y'} - 1)}. \quad (2.27)$$

Substituting for  $Z_{in}$  in Eq. (2.13) we obtain for the inelastic part of  $\Gamma(Y - y)$  (see Fig. 1-b),

$$\Gamma_{in}(Y - y) = \frac{2\tilde{g}\gamma e^{\Delta(Y-y)}}{1 + 2\tilde{g}\gamma e^{\Delta(Y-y)}} = \frac{2L(Y - y)}{1 + 2L(Y - y)}. \quad (2.28)$$

Eq. (2.28) has been derived from the direct summation of the Pomeron diagrams in Ref. [25]. The fact that we reproduce the results of Ref. [25], vindicates our choice of the generating functions in Eq. (2.19) and Eq. (2.20).

Using  $Z_{el}$  we obtain the elastic contribution which is intimately related to the processes of diffraction production:

$$\Gamma_{el}(Y - y) = \frac{2\tilde{g}\gamma e^{\Delta(Y-y)}}{1 + \tilde{g}\gamma e^{\Delta(Y-y)}} - \frac{2\tilde{g}\gamma e^{\Delta(Y-y)}}{1 + 2\tilde{g}\gamma e^{\Delta(Y-y)}} = \frac{2L(Y - y)}{1 + L(Y - y)} - \frac{2L(Y - y)}{1 + 2L(Y - y)}. \quad (2.29)$$

The resulting  $\Gamma(Y - y)$  is given by:

$$\Gamma(Y - y) = \frac{2L(Y - y)}{1 + L(Y - y)}. \quad (2.30)$$

Actually Eq. (2.30) gives the same expression as Eq. (2.6). The difference in an extra factor,  $\sqrt{\gamma}$ , stems from the fact that, we need to take  $\tilde{g}$  rather than  $g$  in the vertex for the Pomeron-hadron interaction.

### 2.4.3 Single inclusive production in MPSI approximation

As one can see from Fig. 1-c, to evaluate the single inclusive cross section, we need to calculate  $\Gamma(Y - y)$ . We have done so in the previous section, however, we now want to take into account both  $L^n(Y - y)$  and  $T^n(Y - y)$  contributions. From Fig. 7-c we see that  $Z(w^{(2)}, \bar{w}^{(2)}, v^{(2)}; Y')$  has the form given in Eq. (2.25). However, in  $Z(w^{(1)}, \bar{w}^{(1)}, v^{(1)}; Y')$ , we need to take into account that each Pomeron at  $Y - Y' = 0$ , creates a cascade of Pomerons that is described by Eq. (2.10). In other words, we need to replace  $w^{(1)}$ ,  $\bar{w}^{(1)}$  and  $v^{(1)}$  in Eq. (2.19) by

$$w^{(1)} \rightarrow \frac{w^{(1)} e^{-\Delta(Y-Y')}}{1 + w^{(1)}(e^{-\Delta(Y-Y')} - 1)}; \quad \bar{w}^{(1)} \rightarrow \frac{\bar{w}^{(1)} e^{-\Delta(Y-Y')}}{1 + \bar{w}^{(1)}(e^{-\Delta(Y-Y')} - 1)}; \quad (2.31)$$

$$v^{(1)} \rightarrow \frac{w^{(1)} e^{-\Delta(Y-Y')}}{1 + w^{(1)}(e^{-\Delta(Y-Y')} - 1)} + \frac{\bar{w}^{(1)} e^{-\Delta(Y-Y')}}{1 + \bar{w}^{(1)}(e^{-\Delta(Y-Y')} - 1)} - \frac{(w^{(1)} + \bar{w}^{(1)} - v^{(1)})e^{-\Delta(Y-Y')}}{1 + (w + \bar{w} - v)(e^{-\Delta(Y-Y')} - 1)}. \quad (2.32)$$

Using these substitutions we obtain

$$Z\left(w^{(1)}, \bar{w}^{(1)}, v^{(1)}; Y - Y'\right) = \exp\left(\frac{(w^{(1)} + \bar{w}^{(1)} - v^{(1)})e^{-\Delta(Y-Y')}}{1 + (w + \bar{w} - v)(e^{-\Delta(Y-Y')} - 1)}\right). \quad (2.33)$$

Using the generating function for Laguerre polynomials (see Ref. [29] formula **8.973(1)**),

$$(1 - z)^{-\alpha-1} \exp\left(\frac{xz}{z-1}\right) = \sum_{n=0}^{\infty} L_n^\alpha(x) z^n. \quad (2.34)$$

We obtain for Eq. (2.33)

$$Z\left(w^{(1)}, \bar{w}^{(1)}, v^{(1)}; Y'\right) = - \sum_{n=0}^{\infty} L_n^{-1}(\tilde{g}_i) \left(-\left(\gamma^{(1)} + \bar{\gamma}^{(1)} - \gamma_{in}^{(1)}\right) e^{\Delta(Y-Y')}\right)^n. \quad (2.35)$$

From Eq. (2.13) using

$$\frac{\partial^l}{\partial^l \gamma^{(1)}} \frac{\partial^m}{\partial^m \bar{\gamma}^{(1)}} \frac{\partial^{n-l-m}}{\partial^{n-l-m} \gamma_{in}^{(1)}} \left(\gamma^{(1)} + \bar{\gamma}^{(1)} - \gamma_{in}^{(1)}\right)^n = (-1)^{n-l-m} n!. \quad (2.36)$$

We obtain

$$\Gamma(Y - y) = \sum_{n=1}^{\infty} L_n^{-1}(\tilde{g}_i) n! (-\gamma e^{\Delta Y})^n = \sum_{n=1}^{\infty} L_n^{-1}(\tilde{g}_i) n! (-1)^n T^n (Y - y). \quad (2.37)$$

Introducing  $n! = \int_0^\infty d\xi \xi^n \exp(-\xi)$  we reduce Eq. (2.37) to the form

$$\Gamma(L(Y - y), T(Y - y)) = \int_0^\infty d\xi e^{-\xi} \left( e^{-\frac{\xi \tilde{g}_i \gamma e^{\Delta(Y-y)}}{1 + \xi \gamma e^{\Delta(Y-y)}}} - 1 \right) = \int_0^\infty d\xi e^{-\xi} \left( e^{-\frac{\xi L(Y-y)}{1 + \xi T(Y-y)}} - 1 \right). \quad (2.38)$$

Using Eq. (2.38) we obtain the following result for the single inclusive cross section:

$$\frac{d\sigma}{dy} = a_P \Gamma(L(Y - y), T(Y - y)) \Gamma(L(y), T(y)), \quad (2.39)$$

where,  $a_P$  denotes the vertex of emission of the hadron from Pomeron (see Fig. 1 and Fig. 2-b).

## 2.5 The Correlation function in MPSI approximation

Calculating  $N(Y - y_1, Y - y_2)$  (see Fig. 1-a) we use  $Z(w^{(1)}, \bar{w}^{(1)}, v^{(1)}; Y - Y')$ , given by Eq. (2.33), as one can see from Fig. 6. However,  $Z(\gamma^{(2)}, \bar{\gamma}^{(2)}, \gamma_{in}^{(2)}|Y')$  is different from the expression which has been used in the calculation of the single inclusive cross section, and it can be written as:

$$Z\left(\gamma^{(2)}, \bar{\gamma}^{(2)}, \gamma_{in}^{(2)}|Y' - y_1, Y' - y_2\right) = \quad (2.40)$$

$$Z\left(\text{Eq. (2.25)}|\gamma^{(2)}, \bar{\gamma}^{(2)}, \gamma_{in}^{(2)}|Y - y_1\right) Z\left(\text{Eq. (2.25)}|\gamma^{(2)}, \bar{\gamma}^{(2)}, \gamma_{in}^{(2)}|Y - y_2\right).$$

First, we calculate  $N(Y - y, Y - y_2)$  at  $y_1 = y_2$ . Using Eq. (2.35) and Eq. (2.36) we obtain from Eq. (2.13) that

$$N(Y - y_1, Y - y_1) = \sum_{n=1}^{\infty} L_n^{-1}(\tilde{g}_i) n! (n-1) (-1)^n T^n (Y - y) \quad (2.41)$$

$$\begin{aligned} &= T^2 \frac{d}{dT} (1/T) \left\{ \sum_{n=1}^{\infty} L_n^{-1}(\tilde{g}_i) n! (-1)^n T^n (Y - y) \right\} \\ &= \int_0^{\infty} d\xi e^{-\xi} \left\{ 1 + e^{-\frac{\xi L(Y-y_1)}{1+\xi T(Y-y_1)}} \left( \frac{-1 - \xi T(Y-y_1) - \xi L(Y-y_1)}{(1 + \xi T(Y-y_1))^2} \right) \right\}. \end{aligned} \quad (2.42)$$

At  $L(Y - y_1) \gg 1$  we expand Eq. (2.42) to estimate the importance of the the correction depending on  $T(Y - y)$ . The first four terms are given by:

$$N(L(Y - y_1), T(Y - y_1); L(Y - y_1), T(Y - y_1)) = \frac{L^2(Y - y_1)}{(1 + L(Y - y_1))^2} \quad (2.43)$$

$$\begin{aligned} &- 4 \frac{L^2(Y - y_1) T(Y - y_1)}{(1 + L(Y - y_1))^4} - 12 \frac{L^3(Y - y_1) T^2(Y - y_1)}{(1 + L(Y - y_1))^6} - 48 \frac{L^4(Y - y_1) T^3(Y - y_1)}{(1 + L(Y - y_1))^8} - \dots \\ &= \frac{L^2(Y - y_1)}{(1 + L(Y - y_1))^2} - 2 \sum_{n=2}^{\infty} n! \frac{L^n(Y - y_1) T^{n-1}(Y - y_1)}{(1 + L(Y - y_1))^{2n}}. \end{aligned} \quad (2.44)$$

Note that all corrections have minus signs and the function of Eq. (2.42) gives the analytical summation of the asymptotic series of Eq. (2.43). For  $y_1 \neq y_2$  we have a more complex answer, namely,

$$\begin{aligned} N(L(Y - y_1), T(Y - y_1); L(Y - y_2), T(Y - y_2)) = & \quad (2.45) \\ & \frac{\left\{ T(Y - y_2) \Gamma(L(Y - y_1), T(Y - y_1)) - T(Y - y_1) \Gamma(L(Y - y_2), T(Y - y_2)) \right\}}{(T(Y - y_2) - T(Y - y_1))}. \end{aligned}$$

The double inclusive cross section can be written as (see Fig. 1-a)

$$\begin{aligned} \frac{d^2\sigma}{dy_1 dy_2} = & \quad (2.46) \\ & \alpha_{\mathbb{P}}^2 N(L(Y - y_1), T(Y - y_1); L(Y - y_1), T(Y - y_1)) N(L(y_1), T(y_1); L(y_1), T(y_1)). \end{aligned}$$

### 3. Correlations in a model for soft interactions

Recently considerable progress has been achieved in building models for soft scattering at high energies [8–13]. The main ingredient of these models is the soft Pomeron with a relatively large intercept  $\Delta_{\mathbb{P}} = \alpha_{\mathbb{P}} - 1 = 0.2 - 0.4$  and exceedingly small slope  $\alpha'_{\mathbb{P}} \simeq 0.02 \text{ GeV}^{-2}$ . Such a Pomeron appears in N=4 SYM [14–18] with a large coupling. This is, at present, is the only theory that allows us to treat the strong interaction on the theoretical basis. Having  $\alpha'_{\mathbb{P}} \rightarrow 0$ , the Pomeron in these models has a natural matching with the hard Pomeron that occurs in perturbative QCD. Therefore, these models could be a

$\Delta_{\mathcal{P}}$	$\beta$	$g_1 (GeV^{-1})$	$g_2 (GeV^{-1})$
0.23	0.46	1.89	61.99
$m_1$ (GeV)	$m_2$ (GeV)	$\gamma$	$G_{3\mathcal{P}}/\Delta_{\mathcal{P}} (GeV^{-1})$
5	1.71	0.0045	0.03

**Table 1:** Fitted parameters for our model.  $\alpha'_{\mathcal{P}} = 0.028 GeV^{-2}$ .

first step in building a selfconsistent theoretical description of the soft interaction at high energy, in spite of its many phenomenological parameters (of the order of 10-15) in every model.

In this section we shall discuss the size of the correlation function in our model [8–10]. This model describes the LHC data (see Refs. [30–33]), including the single inclusive cross section. Thus our next step is to try, to understand the predicted size of the long range rapidity correlations in this model.

### 3.1 Estimates of the rapidity correlation function

In Table 1 we present the main parameters of our model. The parameter  $T(Y) = \gamma e^{\Delta_{\mathcal{P}} Y}$  is small in our model reaching about 0.3 at the LHC energies. However,  $L_i(Y; b) = g_i(b) G_{3\mathcal{P}}/\Delta_{\mathcal{P}} e^{\Delta_{\mathcal{P}} Y}$  is large (see Ref. [8, 9]).

$$g_i(b) = g_i S_i(b) = \frac{g_i}{4\pi} m_i^3 b K_1(m_i b). \quad (3.1)$$

One can see that  $L_2(Y, b=0)$  is as large as 25 at  $Y = 17.7$ . Therefore, we can evaluate the influence of the corrections with respect to  $T(Y)$ , by calculating the contributions of two diagrams: Fig. 4-a (the main contribution) and Fig. 4 - b (the corrections  $\propto T(Y)$ ). We need to use the first two terms of Eq. (2.43) to calculate  $N(L(Y - y_1), T(Y - y_1); L(Y - y_1), T(Y - y_1))$  while being careful to account for the correct  $b$  dependence.

Introducing two functions,

$$\Gamma^{(1)}(L_i(Y - y; b)) = \Delta_{\mathcal{P}} \frac{L_i(Y - y; b)}{1 + L_i(Y - y; b)}; \quad \Gamma^{(2)}(L_i(Y - y; b)) = \Delta_{\mathcal{P}} \frac{L_i(Y - y; b)}{(1 + L_i(Y - y; b))^2}. \quad (3.2)$$

We can see that Fig. 4-a has the following contributions:

$$\begin{aligned} \frac{d^2\sigma^{(0)}}{dy_1 dy_2} &= \int d^2b \left\{ \int d^2b' \Gamma^{(1)}(L_i(Y - y_1; \vec{b}')) \Gamma^{(1)}(L_i(y_1; \vec{b} - \vec{b}')) \right\} \\ &\times \left\{ \int d^2b' \Gamma^{(1)}(L_i(Y - y_1; \vec{b}')) \Gamma^{(1)}(L_i(y_2; \vec{b} - \vec{b}')) \right\}, \end{aligned} \quad (3.3)$$

while for Fig. 4-b we have, for  $y_1 > y_2$ :

$$\begin{aligned} \frac{d^2\sigma^{(1)}}{dy_1 dy_2} &= -4T(Y - y_1) \\ &\times \int d^2b d^2b' \Gamma^{(2)}(L_i(Y - y_1; \vec{b} - \vec{b}')) \Gamma^{(2)}(L_i(Y - y_2; \vec{b} - \vec{b}')) \Gamma^{(1)}(L_i(y_1; \vec{b}')) \Gamma^{(1)}(L_i(y_2; \vec{b}')) \end{aligned} \quad (3.4)$$

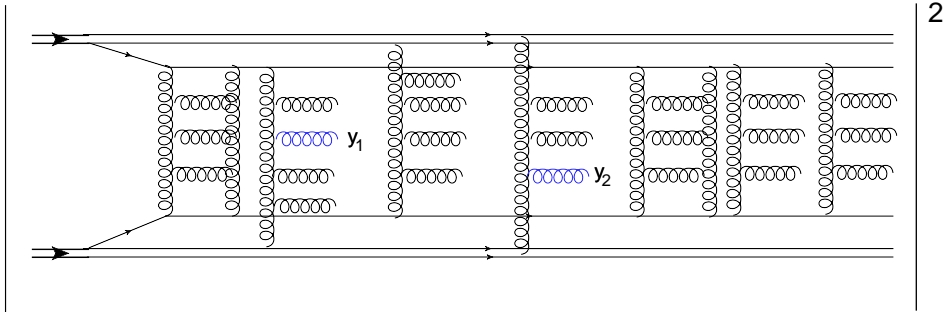


**Figure 8:** The general diagram for the production of two hadrons(gluons) with rapidities  $y_1$  and  $y_2$ .

Performing the calculations, we found that the correlation function  $R(y_1 = Y/2, y_2 = Y/2)$  (see Eq. (1.5)) is equal to  $R^{(0)}(y_1 = Y/2, y_2 = Y/2) = 13$  at the Tevatron energy and  $R^{(0)}(y_1 = Y/2, y_2 = Y/2) = 16$  at  $W = 7TeV$ . The corrections turn out to be small ( $< 5\%$ ) for both energies. Indeed, large correlations were not seen at Tevatron.

### 3.2 Improvement of the model

Eq. (3.3) is written without taking into account any corrections due to energy conservation. As has been discussed in the 80'th (see Refs. [35,36]), these corrections are important for the calculation of the correlations. Generally speaking, in Pomeron calculus the long range correlations in rapidity stem from the production of two hadrons from two different Pomerons (two different parton showers, see Fig. 8). In other words, two hadrons in the central rapidity region can be produced in an event with more than two parton showers (see Fig. 8). This is shown in Fig. 7-a in an eikonal type model, where the proton-proton scattering amplitude is written as:

$$A(s, b) = i \left( 1 - e^{-\frac{1}{2}\Omega(s, b)} \right). \quad (3.5)$$

The cross section of  $n$  parton showers production is equal to (see Refs. [35,36] and references therein)

$$\sigma_{n\text{-showers}} = \int d^2b \frac{\Omega^n(s, b)}{n!} e^{-\Omega(s, b)}. \quad (3.6)$$

Eq. (3.6) shows that the parton showers are distributed according to Poisson distribution with an average number of parton showers  $\Omega(s, b)$  which has the following form in the simple model of Eq. (3.5):

$$\Omega(s, b) = \int d^2b' g(b') g(\vec{b} - \vec{b}') \left( \frac{s}{s_0} \right)^{\Delta_P}. \quad (3.7)$$

However, the simple Eq. (3.6) has to be modified to account for the fact that the energy of the parton shower is not equal to  $W = \sqrt{s}$ , but it is smaller or equal to  $\tilde{W} = \sqrt{x_1 x_2 s}$  (see Fig. 9). The easiest way

to find  $x_1$  and  $x_2$  is to assume that both  $p_1^2 = p_2^2 = -\bar{Q}^2 \gg \mu_{\text{soft}}^2$ , where  $\mu_{\text{soft}}$  is the scale of the soft interactions  $\mu_{\text{soft}} \sim \Lambda_{QCD}$ . In Ref. [37] we have argued that for a Pomeron  $\bar{Q}^2 \approx 2 GeV^2 \gg \mu_{\text{soft}}$ . Bearing this in mind, the energy variable  $x_1$  ( $x_2$ ) for gluon-hadron scattering is equal to

$$0 = (x_1 P_1 + p_1)^2 = -\bar{Q}^2 + x_1 2 p_1 \cdot P_1; \quad p_1^2 = -\bar{Q}^2; \quad x_1 = \frac{\bar{Q}^2}{M^2 + \bar{Q}^2}. \quad (3.8)$$

$p_1$ ,  $P_1$  and  $x_1 P_1$  are the momenta of the gluon, the hadron and the parton (quark or gluon) with which the initial gluon interacts. From Eq. (3.8) one can see that

$$\tilde{s} = x_1 x_2 S = \frac{s \bar{Q}^4}{M^4} \quad (3.9)$$

For the second parton shower  $\tilde{s} = (q_1 + q_2)^2$  (see Fig. 9), where  $q_i = (x_1^{q_i} P_1, x_2^{q_i} P_2, \vec{q}_{i,\perp})$ . Using

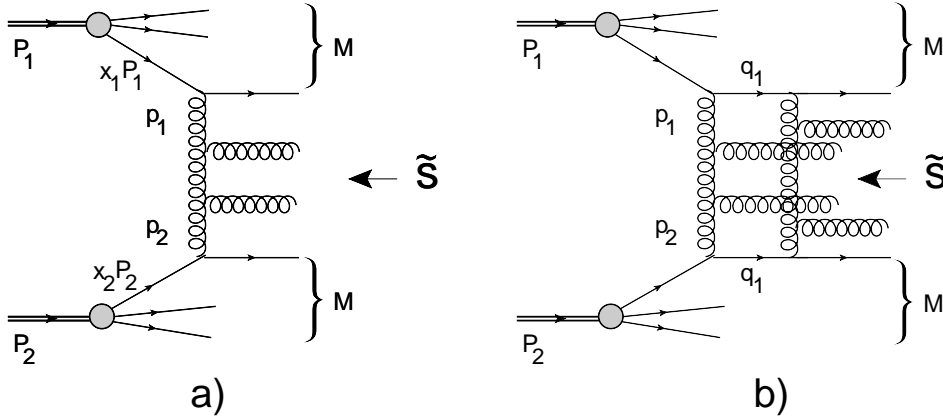


**Figure 9:** Production of one (Fig. 9-a) and two (Fig. 9-b) parton showers.

the conservation of momentum we see that  $x_1^{g_1} = x_1 + x_1^{g_1}$  and  $x_2^{g_2} = x_2 + x_2^{g_2}$ . Note that  $g_1$  and  $g_2$  denote the gluons with momenta  $p_1$  and  $p_2$  respectively (see Fig. 9). Vectors  $p_1$  and  $p_2$  take the form:  $p_1 = (x_1^{g_1} P_1, x_2^{g_1} P_2, \vec{p}_{1,\perp})$  and  $p_2 = (x_1^{g_2} P_1, x_2^{g_2} P_2, \vec{p}_{2,\perp})$ . Bear in mind the following equations:

$$(p_1 + P_1)^2 = M^2; \quad x_2^{g_1} = \frac{M^2}{s}; \quad p_1^2 = x_1^{g_1}, x_2^{g_1} s + p_{1,\perp}^2 = \bar{Q}^2; \quad x_1^{g_1} < \frac{\bar{Q}^2}{x_2^{g_1} s} = \frac{\bar{Q}^2}{M^2} \ll x_1. \\ (p_2 + P_2)^2 = M^2; \quad x_1^{g_2} = \frac{M^2}{s}; \quad p_2^2 = x_2^{g_2}, x_1^{g_2} s + p_{2,\perp}^2 = \bar{Q}^2; \quad x_2^{g_2} < \frac{\bar{Q}^2}{x_1^{g_2} s} = \frac{\bar{Q}^2}{M^2} \ll x_2 \quad (3.10)$$

Therefore, the value of  $\tilde{s}$  for the second parton shower turns out to be the same as for the first one for  $M^2 \gg \bar{Q}^2$ . The value of  $M$  can be estimated using the quark structure function as it has been suggested in Ref. [37]. Indeed,

$$\langle |M^2| \rangle = \frac{\int \frac{dM^2}{M^2} M^2 q\left(\frac{\bar{Q}^2}{M^2 + \bar{Q}^2}, \bar{Q}^2\right)}{\int \frac{dM^2}{M^2} q\left(\frac{\bar{Q}^2}{M^2 + \bar{Q}^2}, \bar{Q}^2\right)}. \quad (3.11)$$

Using  $\bar{Q} = 1 \text{ GeV}$  and  $q(x, \bar{Q}^2)$  given by a combined fit [38] of H1 and ZEUS data (HERAPDF01) we obtain that  $\langle |M^2| \rangle \approx 87 \text{ GeV}^2$  which is much larger than  $\bar{Q}^2$ .

However, the scale of hardness  $\bar{Q}$  in CGC/saturation approach is proportional to the saturation momentum  $Q_s$  ( $\bar{Q} \propto Q_s$ ) and, therefore, depends on energy. Such energy dependence of  $\bar{Q}$  induces the dependence of average mass  $M$  on energy. Assuming that  $Q_s^2 \propto s^\lambda$  with  $\lambda = 0.24$  we found that in the energy range  $W = 0.9 \div 7 \text{ TeV}$  the typical  $M^2 = M_0^2(W = 0.9 \text{ TeV}) s^\beta$  with  $\beta = 0.07$ .

Taking into account Eq. (3.9) one can re-write Eq. (3.6) in the form  $\langle |M^2| \rangle = M_0^2 \left( \frac{s}{s_0} \right)^\beta$  with  $\beta = 0.14$  and  $\sqrt{s_0} = 0.9 \text{ TeV}$ .  $M_0$  is equal to  $10 \text{ GeV}$ .

$$\sigma_{n\text{-showers}}(s) = \int d^2b \frac{\Omega^n(\tilde{s}, b)}{n!} e^{-\Omega(s, b)}. \quad (3.12)$$

We need to sum over  $n \geq 2$  to get the double inclusive production cross section,

$$\frac{d^2\sigma}{dy_1 dy_2} = 2 a_{\mathcal{P}}^2 \sum_{n=2} \sigma_{n\text{-showers}}(s) = a_{\mathcal{P}}^2 \int d^2b \Omega^2(\tilde{s}, b) e^{\Omega(\tilde{s}, b) - \Omega(s, b)}, \quad (3.13)$$

where,  $a_{\mathcal{P}}$  is a new vertex defined as shown in Fig. 2-b). The factor 2 stems from the possibility to emit a hadron with rapidity  $y_1$  from each of two parton showers. One can see that the double inclusive cross section does not depend on  $y_1$  and  $y_2$ , leading to the long range rapidity correlation.

### 3.3 Rapidity long range correlations in GLM model for soft interactions at high energy

In the model for soft interactions that has been suggested in Refs. [8–10] (GLM model) we evaluate more complicated sum of diagrams than in Eq. (3.5). The different contributions to the two particle correlation in this model are shown in Fig. 10.

#### 3.3.1 The main ingredients of the GLM model

*Eikonal diagrams:*

In order to account for diffraction dissociation in the states with masses that are much smaller than the initial energy, we use the simple two channel Good-Walker model. In this model we introduce two eigen wave functions,  $\psi_1$  and  $\psi_2$ , which diagonalize the 2x2 interaction matrix  $\mathbf{T}$ ,

$$A_{i,k} = \langle \psi_i \psi_k | \mathbf{T} | \psi_{i'} \psi_{k'} \rangle = A_{i,k} \delta_{i,i'} \delta_{k,k'}. \quad (3.14)$$

The two observed states are an hadron whose wave function we denote by  $\psi_h$ , and a diffractive state with a wave function  $\psi_D$ , which is the sum of all the Fock diffractive states. These two observed states can be written in the form

$$\psi_h = \alpha \psi_1 + \beta \psi_2, \quad \psi_D = -\beta \psi_1 + \alpha \psi_2, \quad (3.15)$$

where,  $\alpha^2 + \beta^2 = 1$ . For each state we sum the eikonal diagrams of Fig. 7-a using Eq. (3.5). The first contribution to  $\Omega(s, b)$  is the exchange of a single Pomeron. However, the Pomeron interaction leads to a more complicated expression for  $\Omega(s, b)$ .

*Enhanced diagrams:*

In our model [10], the Pomeron's Green function which includes all enhanced diagrams, is approximated using the MPSI procedure [23], in which a multi Pomeron interaction (taking into account only triple Pomeron vertices) is approximated by large Pomeron loops of rapidity size of  $\ln s$ . We obtain

$$G_{\mathcal{P}}(Y) = 1 - \exp\left(\frac{1}{T(Y)}\right) \frac{1}{T(Y)} \Gamma\left(0, \frac{1}{T(Y)}\right), \quad (3.16)$$

in which:

$$T(Y) = \gamma e^{\Delta_{\mathcal{P}} Y}. \quad (3.17)$$

$\Gamma(0, 1/T)$  is the incomplete gamma function (see formulae **8.35** in Ref. [29]).

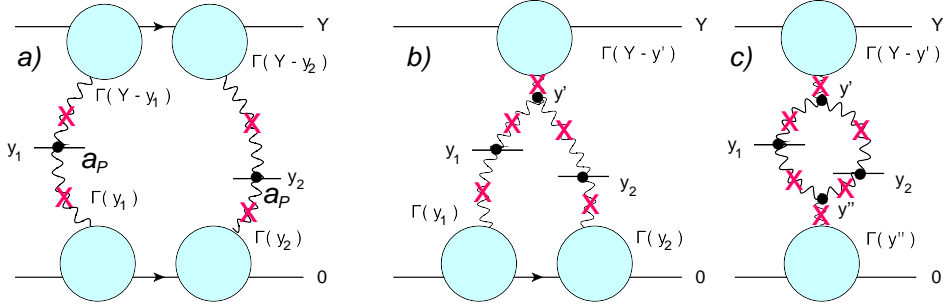


**Figure 10:** Mueller diagrams for double inclusive production in the GLM model [8–10]. Crosses mark the cut Pomerons.  $\Gamma(y)$  is given by Eq. (2.6). All rapidities are in the laboratory reference frame.

*Semi-enhanced (net) diagrams:*

A brief glance at the values of the parameters of our model (see Ref. [8] and Table 1), shows that we have a new small parameter,  $T(Y) = G_{3\mathcal{P}}^2 (s/s_0)^{\Delta_{\mathcal{P}}} \ll 1$ , while,  $L_i(Y, b) = G_{3\mathcal{P}} g_i(b) (s/s_0)^{\Delta_{\mathcal{P}}} \approx 1$ . We call the diagrams which are proportional to  $L_i^n(Y, b)$ , but do not contain any of the  $T^n(Y, b)$  contributions, net diagrams. Summing the net diagrams [9], we obtain the following expression for  $\Omega_{\mathcal{P}}^{i,k}(s, b)$ :

$$\Omega_{\mathcal{P}}^{i,k}(Y; b) = \int d^2 b' \frac{g_i(\vec{b}') g_k(\vec{b} - \vec{b}') (1/\gamma G_{\mathcal{P}}(T(Y)))}{1 + (G_{3\mathcal{P}}/\gamma) G_{\mathcal{P}}(T(Y)) [g_i(\vec{b}') + g_k(\vec{b} - \vec{b}')]} \quad (3.18)$$

$G_{3\mathcal{P}}$  is the triple Pomeron vertex, and  $\gamma^2 = \int \frac{d^2 k_t}{4\pi^2} G_{3\mathcal{P}}^2$ .

### 3.3.2 Formulae for the double inclusive cross section

Mueller diagrams for the different contributions to the double inclusive production are shown in Fig. **10**. The diagram of Fig. **10**-a is the same as we have discussed in section 3.1. The main ingredient for this contribution is  $\Gamma_i(Y; b)$ , which is given by a slight modification of Eq. (3.2):

$$\Gamma_i(Y - y, b) = \frac{g_i(b) \frac{1}{\gamma} G_{\mathcal{P}}(T(Y - y))}{1 + (G_{3\mathcal{P}}/\gamma) g_i(b) G_{\mathcal{P}}(T(Y - y))}. \quad (3.19)$$

Introducing,

$$H_{ik}(Y_1; Y_2; b) \equiv \int d^2b' \Gamma_i(\vec{b} - \vec{b}', Y_1) \Gamma_k(\vec{b}', Y_2), \quad (3.20)$$

we can rewrite the contribution of the diagram of Fig. 10-a in the form

$$\begin{aligned} I_2(y_1, y_2) = & \\ & a_{\mathcal{P}}^2 \left( \int d^2b \left\{ \alpha^4 \exp\left(\Omega_{11}(\tilde{Y}; b) - \Omega_{11}(Y; b)\right) H_{11}\left(\tilde{Y}/2 - y_1, \tilde{Y}/2 + y_1; b\right) H_{11}\left(\tilde{Y}/2 - y_2, \tilde{Y}/2 + y_2; b\right) \right. \right. \\ & + 2\alpha^2 \beta^2 \exp\left(\Omega_{12}(\tilde{Y}; b) - \Omega_{12}(Y; b)\right) H_{12}\left(\tilde{Y}/2 - y_1, \tilde{Y}/2 + y_1; b\right) H_{12}\left(\tilde{Y}/2 - y_1, \tilde{Y}/2 + y_1; b\right) \\ & \left. \left. + \beta^4 \exp\left(\Omega_{22}(\tilde{Y}; b) - \Omega_{22}(Y; b)\right) H_{22}\left(\tilde{Y}/2 - y_1, \tilde{Y}/2 + y_1; b\right) H_{22}\left(\tilde{Y}/2 - y_1, \tilde{Y}/2 + y_1; b\right) \right\}, \quad (3.21) \end{aligned}$$

where,  $a_{\mathcal{P}}$  is shown in Fig. 2. In Eq. (3.21) we used the following notations:  $Y = \ln(s/s_0)$  and  $\tilde{Y} = \ln(\tilde{s}/s_0)$ .  $y_1$  and  $y_2$  are rapidities of the produced hadrons in the c.m.frame. For the contribution of the diagram of Fig. 10-b, we need to change  $H_{ik}(\tilde{Y}/2 - y_1, \tilde{Y}/2 + y_1; b)$  in Eq. (3.21) to  $J_{ik}(y_1, y_2; b)$  which is defined as

$$\begin{aligned} J_{ik}(y_1, y_2; b) = & \int_{\tilde{Y}/2 - y_1}^{\tilde{Y}} dy' \int d^2b' \Gamma_i(\tilde{Y} - y'; \vec{b} - \vec{b}') G_{\mathcal{P}}\left(T(y' - \tilde{Y}/2 + y_1)\right) G_{\mathcal{P}}\left(T(y' - \tilde{Y}/2 + y_2)\right) \\ & \times \Gamma_k(\tilde{Y}/2 - y_1, b') \Gamma_k(\tilde{Y}/2 - y_2, b'). \quad (3.22) \end{aligned}$$

Therefore, this contribution takes the form

$$\begin{aligned} I_1(y_1, y_2) = & a_{\mathcal{P}}^2 G_{3\mathcal{P}} \int d^2b \left\{ \alpha^4 \exp\left(\Omega_{11}(\tilde{Y}; b) - \Omega_{11}(Y; b)\right) J_{11}(y_1, y_2; b) \right. \\ & \left. + 2\alpha^2 \beta^2 \exp\left(\Omega_{12}(\tilde{Y}; b) - \Omega_{12}(Y; b)\right) J_{12}(y_1, y_2; b) + \beta^4 \exp\left(\Omega_{22}(\tilde{Y}; b) - \Omega_{22}(Y; b)\right) J_{22}(y_1, y_2; b) \right\}. \quad (3.23) \end{aligned}$$

Introducing,

$$\begin{aligned} K_{ik}(y_1, y_2; b) = & \int d^2b' \int_{\tilde{Y}/2 - y_1}^{\tilde{Y}} dy' \Gamma_i(\tilde{Y} - y'; \vec{b} - \vec{b}') G_{\mathcal{P}}\left(T(y' - \tilde{Y}/2 + y_1)\right) G_{\mathcal{P}}\left(T(y' - \tilde{Y}/2 + y_2)\right) \\ & \times \int_0^{\tilde{Y}/2 - y_2} dy'' \Gamma_k(y''; \vec{b} - \vec{b}') G_{\mathcal{P}}\left(T(\tilde{Y}/2 - y_1 - y'')\right) G_{\mathcal{P}}\left(T(\tilde{Y}/2 - y_2 - y'')\right). \quad (3.24) \end{aligned}$$

We can reduce the contribution of the diagram of Fig. 10-c to the form

$$\begin{aligned} I_3(y_1, y_2) = & a_{\mathcal{P}}^2 G_{3\mathcal{P}}^2 \int d^2b \left\{ \alpha^4 \exp\left(\Omega_{11}(\tilde{Y}; b) - \Omega_{11}(Y; b)\right) K_{11}(y_1, y_2; b) \right. \\ & \left. + 2\alpha^2 \beta^2 \exp\left(\Omega_{12}(\tilde{Y}; b) - \Omega_{12}(Y; b)\right) K_{12}(y_1, y_2; b) + \beta^4 \exp\left(\Omega_{22}(\tilde{Y}; b) - \Omega_{22}(Y; b)\right) K_{22}(y_1, y_2; b) \right\}. \quad (3.25) \end{aligned}$$

Collecting all contributions, the long range rapidity correlation function has the following form:

W(TeV)	0.9	1.8	2.36	7
$R(y_1 = 0, y_2 = 0)$	1.0	1.12	1.026	1.034

**Table 2:**  $R(y_1 = 0, y_2 = 0)$  versus energy.

$$R(\eta_1, \eta_2) = \frac{h^2(\eta, Q)}{\sigma_{in}(Y(\eta))} \{I_1(y_1(\eta_1), y_1(\eta_2)) + I_2(y_1(\eta_1), y_1(\eta_2)) + I_3(y_1(\eta_1), y_1(\eta_2))\} \frac{1}{\sigma_{in}(Y)} \frac{d\sigma}{dy_1} \frac{1}{\sigma_{in}(Y)} \frac{d\sigma}{dy_1} - 1. \quad (3.26)$$

Expressions for the single inclusive cross section  $\frac{1}{\sigma_{in}(Y)} \frac{d\sigma}{dy_i}$  as well as the Jacobian  $h$  and the definition of the pseudo-rapidity  $\eta$  can be found in Ref. [39].

### 3.3.3 Correlations in the GLM model

Using the formulae of the previous section we calculate the correlations in the GLM model. It turns out that  $R(0, 0)$  is a constant in the energy range  $W = 0.9$  to  $7$  TeV, and it is equal to  $R(0, 0) \approx 2$  (see Table 2). This result is in a good agreement with the CMS data on multiplicity distribution [40]. Indeed, experimentally,  $C_2 = \langle n^2 \rangle / \langle n \rangle^2$  was measured for the rapidity window  $|\eta| < 0.5$  in the energy range  $W = 0.9$  to  $7$  TeV (see Fig.6 in Ref. [40]) and  $C_2 \approx 2$ . For this small range of rapidity, we can consider that  $C_2 = R(0, 0) + 1$ . It is worthwhile mentioning that using our calculation of  $R(0, 0)$ , we can calculate the parameters of the negative binomial distribution

$$\frac{\sigma_n}{\sigma_{in}} = \left( \frac{r}{r + \langle n \rangle} \right)^r \frac{\Gamma(n + r)}{n! \Gamma(r)} \left( \frac{\langle n \rangle}{r + \langle n \rangle} \right)^n. \quad (3.27)$$

In our model, given  $|\eta| \leq 0.5$ ,  $\langle n \rangle = 5.8$  (see Ref. [39]) and  $r = 1.25$ . Using this distribution we calculate  $C_q = \langle n^q \rangle / \langle n \rangle^q$ . They equal  $C_3 = 5.65$ ,  $C_4 = 21.18$  and  $C_4 = 98.2$ . They are in good agreement with the experimental data of Ref. [40] except  $C_4$  which experimentally is about 70. In Fig. 11 we compare Eq. (3.27) with the CMS experimental data at  $W = 7$  TeV. In Fig. 12 we plot the correlation function  $R(\eta_1, \eta_2)$  as a function of  $\eta_2$ . One can see that this function falls steeply at large  $\eta_2$ . At first sight, such form of  $\eta_2$  dependence looks strange since all diagrams of Fig. 10 generate long range rapidity correlations. It turns out that the main contribution comes from the enhanced diagram of Fig. 10-c. The eikonal-type diagram of Fig. 10-a leads to long range rapidity correlations which do not depend on the values of  $\eta_1$  and  $\eta_2$ . The diagram of Fig. 10-b gives a negligible contribution. Let us consider Fig. 10-c in a simple model replacing  $\Gamma(y)$  by the exchange of the Pomeron, and considering all Pomeron exchanges as the exchange of a ‘bare’ Pomeron. In this model the diagram of Fig. 10 has the form:

$$\begin{aligned} & g_p^2 a_{\mathbb{P}}^2 G_{3\mathbb{P}}^2 \int_{y_1}^Y dy'' \int_0^{y_2} dy''' G_{\mathbb{P}}(Y - y') G_{\mathbb{P}}(y' - y_1) G_{\mathbb{P}}(y' - y_1) G_{\mathbb{P}}(y' - y_2) \\ & \times G_{\mathbb{P}}(y_2 - y''') G_{\mathbb{P}}(y_2 - y''') G_{\mathbb{P}}(y''') = \\ & g_p^2 a_{\mathbb{P}}^2 \frac{G_{3\mathbb{P}}^2}{\Delta_{\mathbb{P}}^2} e^{2\Delta_{\mathbb{P}} Y} \left( 1 - e^{\Delta_{\mathbb{P}}(y_1 - Y)} - e^{\Delta_{\mathbb{P}}(y_1 - Y)} - e^{\Delta_{\mathbb{P}}(-y_2)} + e^{\Delta_{\mathbb{P}}(y_1 - y_2 - Y)} \right), \end{aligned} \quad (3.28)$$

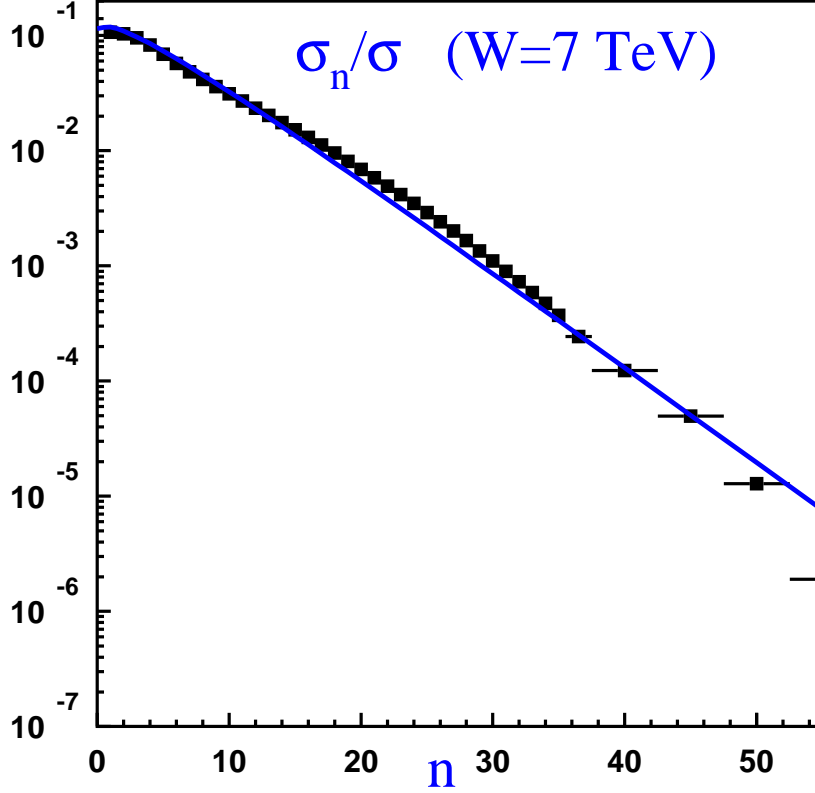


**Figure 11:** Multiplicity distribution measured by CMS collaboration [40] and Eq. (3.27) with our parameters.

where, we used  $G_P(Y) = \exp(\Delta_P Y)$ . Recalling that the single inclusive cross section  $d\sigma/dy = g_p^2 a_p^2 \exp(\Delta_P Y)$ , in this simple model, the correlation function of Eq. (1.5) is equal to

$$R(y_1, y_2) = \sigma_{in} \frac{G_{3P}^2}{\Delta_P^2} \left( 1 - e^{\Delta_P(y_1-Y)} - e^{\Delta_P(y_1-Y)} - e^{\Delta_P(-y_2)} + e^{\Delta_P(y_1-y_2-Y)} \right) - 1. \quad (3.29)$$

In Fig. 12-b the correlation function is plotted with  $\sigma_{in} G_{3P} / \Delta_P^2 = 2$  and  $\Delta_P = 0.08$  which correspond to the effective behaviour of the dressed Pomeron in our model at high energies ( $W = 1.8 - 7 TeV$ ). One can see that simple formula of Eq. (3.29) reproduces the short-range correlation type behaviour of Fig. 12-a.

#### 4. Conclusions

In this paper we taken the next step, following the single inclusive cross section [39], in the description of the multi particle production processes in the framework of our soft interaction model. The main ingredients

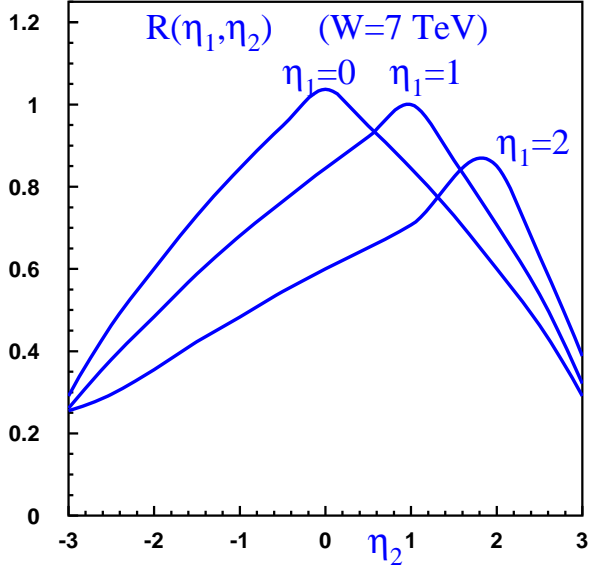


Fig. 12-a

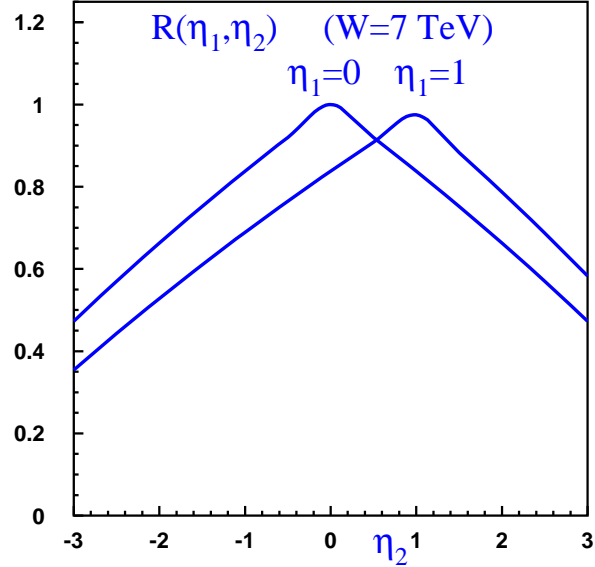


Fig. 12-b

**Figure 12:** Our prediction for  $R(\eta_1, \eta_2)$  versus  $\eta_2$  at different values of  $\eta_1$  at  $W = 7 \text{ TeV}$  (Fig. 12-a) and the estimates of the simple model (see Eq. (3.28) with  $\Delta_P = 0.08$ ) for the correlation function (Fig. 12-b).

of our model are the large Pomeron intercept ( $\Delta_P = 0.23$ ) and  $\alpha'_P = 0$ . The model gives a practical realization of the BFKL Pomeron Calculus in zero transverse dimensions. The model reproduces quite well all classical soft scattering data: total, elastic and diffractive cross sections and the energy dependence of the elastic slope in wide range of energy  $W = 20 \text{ GeV}$  to  $7 \text{ TeV}$ . The attraction of the Pomeron approach reveals itself in the possibility to discuss not only the forward scattering data but, also, to make predictions relating to multiparticle production processes using the AGK cutting rules [21].

In this paper we have developed a procedure for calculating the correlation function in the MPSI approximation utilizing the BFKL Pomeron Calculus in zero transverse dimensions. The theoretical formulae obtained allow us to calculate the rapidity correlation function in our model for soft interactions. We compare our prediction with the multiplicity distribution at  $W = 7 \text{ TeV}$  measured by CMS collaboration [40], which we describe quite well. In Fig. 12 we present our prediction for the rapidity dependence of the correlation function.

We believe that our approach opens the way to discuss the structure of the bias events without building Monte Carlo codes. At the moment we demonstrate that our model describes all standard soft data on forward scattering, inclusive cross sections and multiplicity distribution. We also predict the rapidity correlation function.

We thank all participants of “Low  $x$ ’2013 WS” for fruitful discussions on the subject. This research of E.L. was supported by the Fondecyt (Chile) grant 1100648.

## References

- [1] M. A. Braun, Phys. Lett. **B632** (2006) 297 [arXiv:hep-ph/0512057]; Eur. Phys. J. **C16**, 337 (2000) [arXiv:hep-ph/0001268]; Phys. Lett. B **483** (2000) 115 [arXiv:hep-ph/0003004]; Eur. Phys. J. C **33** (2004) 113 [arXiv:hep-ph/0309293]; **C6**, 321 (1999) [arXiv:hep-ph/9706373]; M. A. Braun and G. P. Vacca, Eur. Phys. J. **C6**, 147 (1999) [arXiv:hep-ph/9711486]
- [2] F. E. Low, Phys. Rev. D **12** (1975) 163; S. Nussinov, Phys. Rev. Lett. **34** (1975) 1286; E. A. Kuraev, L. N. Lipatov, and F. S. Fadin, Sov. Phys. JETP **45**, 199 (1977); Ya. Ya. Balitsky and L. N. Lipatov, Sov. J. Nucl. Phys. **28**, 22 (1978); A. H. Mueller, Nucl. Phys. **B415**, 373 (1994); **B437**, 107 (1995); L. V. Gribov, E. M. Levin and M. G. Ryskin, Phys. Rep. **100**, 1 (1983); A. H. Mueller and J. Qiu, Nucl. Phys.,427 **B 268** (1986) ; L. McLerran and R. Venugopalan, Phys. Rev. **D 49**,2233, 3352 (1994); **D 50**,2225 (1994); **D 53**,458 (1996); **D 59**,09400 (1999); L. N. Lipatov, Phys. Rept. **286**, 131 (1997) [arXiv:hep-ph/9610276]; Sov. Phys. JETP **63**, 904 (1986) and references therein.
- [3] J. Bartels and K. Kutak, Eur. Phys. J. C **53** (2008) 533 [arXiv:0710.3060 [hep-ph]]; J. Bartels, M. Braun and G. P. Vacca, Eur. Phys. J. **C40**, 419 (2005) [arXiv:hep-ph/0412218]; J. Bartels and C. Ewerz, JHEP **9909**, 026 (1999) [arXiv:hep-ph/9908454]; J. Bartels and M. Wusthoff, Z. Phys. **C6Eur. Phys. J. 6**, 157 (1995); A. H. Mueller and B. Patel, Nucl. Phys. **B425**, 471 (1994) [arXiv:hep-ph/9403256]; J. Bartels, Z. Phys. **C60**, 471 (1993).
- [4] A. H. Mueller, Nucl. Phys. **B 415** (1994) 373; **B 437** (1995) 107.
- [5] I. Balitsky, [arXiv:hep-ph/9509348]; *Phys. Rev.* **D60**, 014020 (1999) [arXiv:hep-ph/9812311]; Y. V. Kovchegov, *Phys. Rev.* **D60**, 034008 (1999), [arXiv:hep-ph/9901281].
- [6] Y. V. Kovchegov and E. Levin, Nucl. Phys. B **577** (2000) 221 [hep-ph/9911523].
- [7] J. Jalilian-Marian, A. Kovner, A. Leonidov and H. Weigert, *Phys. Rev.* **D59**, 014014 (1999), [arXiv:hep-ph/9706377]; *Nucl. Phys.* **B504**, 415 (1997), [arXiv:hep-ph/9701284]; J. Jalilian-Marian, A. Kovner and H. Weigert, *Phys. Rev.* **D59**, 014015 (1999), [arXiv:hep-ph/9709432]; A. Kovner, J. G. Milhano and H. Weigert, *Phys. Rev.* **D62**, 114005 (2000), [arXiv:hep-ph/0004014]; E. Iancu, A. Leonidov and L. D. McLerran, *Phys. Lett.* **B510**, 133 (2001); [arXiv:hep-ph/0102009]; *Nucl. Phys.* **A692**, 583 (2001), [arXiv:hep-ph/0011241]; E. Ferreira, E. Iancu, A. Leonidov and L. McLerran, *Nucl. Phys.* **A703**, 489 (2002), [arXiv:hep-ph/0109115]; H. Weigert, *Nucl. Phys.* **A703**, 823 (2002), [arXiv:hep-ph/0004044].
- [8] E. Gotsman, E. Levin and U. Maor, Phys. Lett. B **716** (2012) 425, arXiv:1208.0898 [hep-ph], Phys. Rev. D **85** (2012) 094007, [arXiv:1203.2419 [hep-ph]].
- [9] E. Gotsman, E. Levin and U. Maor, Eur. Phys. J. C **71** (2011) 1553, [arXiv:1010.5323 [hep-ph]].
- [10] E. Gotsman, E. Levin, U. Maor and J. S. Miller, Eur. Phys. J. C **57** (2008) 689 [arXiv:0805.2799 [hep-ph]].
- [11] A. B. Kaidalov and M. G. Poghosyan, arXiv:0909.5156 [hep-ph].
- [12] A. D. Martin, M. G. Ryskin and V. A. Khoze, arXiv:1110.1973 [hep-ph].
- [13] S. Ostapchenko, Phys. Rev. D **83** (2011) 014018 [arXiv:1010.1869 [hep-ph]].
- [14] R. C. Brower, J. Polchinski, M. J. Strassler and C. I. Tan JHEP **0712** (2007) 005 [arXiv:hep-th/0603115]; R. C. Brower, M. J. Strassler and C. I. Tan, "On The Pomeron at Large 't Hooft Coupling", arXiv:0710.4378 [hep-th].

- [15] Y. Hatta, E. Iancu and A. H. Mueller, JHEP **0801** (2008) 026 [arXiv:0710.2148 [hep-th]].
- [16] L. Cornalba and M. S. Costa, Phys. Rev. **D 78**, (2008) 09010, arXiv:0804.1562 [hep-ph]; L. Cornalba, M. S. Costa and J. Penedones, JHEP **0806** (2008) 048 [arXiv:0801.3002 [hep-th]]; JHEP **0709** (2007) 037 [arXiv:0707.0120 [hep-th]].
- [17] B. Pire, C. Roiesnel, L. Szymanowski and S. Wallon, Phys. Lett. B **670**, 84 (2008) [arXiv:0805.4346 [hep-ph]].
- [18] E. Levin, J. Miller, B. Z. Kopeliovich and I. Schmidt, JHEP **0902** (2009) 048; arXiv:0811.3586 [hep-ph].
- [19] P.D.B. Collins, *"An introduction to Regge theory and high energy physics"*, Cambridge University Press 1977; Luca Caneschi (editor), *"Regge Theory of Low- $p_T$  Hadronic Interaction"*, North-Holland 1989 and references therein.
- [20] A. H. Mueller, Phys. Rev. D **2** (1970) 2963.
- [21] V. A. Abramovsky, V. N. Gribov and O. V. Kancheli, *Yad. Fiz.* **18**, 595 (1973) [*Sov. J. Nucl. Phys.* **18**, 308 (1974)].
- [22] J. Jalilian-Marian and Y. V. Kovchegov, Phys. Rev. D **70**, 114017 (2004) [Erratum-ibid. D **71**, 079901 (2005)] [hep-ph/0405266].
- [23] A. H. Mueller and B. Patel: *Nucl. Phys.* **B425** (1994) 471; A. H. Mueller and G. P. Salam: *Nucl. Phys.* **B475**, (1996) 293; G. P. Salam: *Nucl. Phys.* **B461** (1996) 512; E. Iancu and A. H. Mueller: *Nucl. Phys.* **A730** (2004) 460.
- [24] A. Schwimmer, Nucl. Phys. B **94** (1975) 445.
- [25] K. G. Boreskov, A. B. Kaidalov, V. A. Khoze, A. D. Martin and M. G. Ryskin, Eur. Phys. J. **C44** (2005) 523 [arXiv:hep-ph/0506211].
- [26] E. Levin and M. Lublinsky, Nucl. Phys. A730, 191 (2004) [arXiv:hep-ph/0308279], Phys. Lett. B607, 131 (2005) [arXiv:hep-ph/0411121].
- [27] E. Levin and A. Prygarin, Eur. Phys. J. C **53** (2008) 385 [hep-ph/0701178].
- [28] R.J. Glauber, In: Lectures in Theor. Phys., v. 1, ed. W.E. Brittin and L.G. Duham. NY: Intersciences, 1959; V. N. Gribov, Sov. Phys. JETP **29** (1969) 483 [Zh. Eksp. Teor. Fiz. **56** (1969) 892].
- [29] I. Gradstein and I. Ryzhik, *"Tables of Series, Products, and Integrals"*, Verlag MIR, Moskau, 1981.
- [30] M. G. Poghosyan, J. Phys. G **G 38**, 124044 (2011) [arXiv:1109.4510 [hep-ex]]. ALICE Collaboration, *"First proton-proton collisions at the LHC as observed with the ALICE detector: measurement of the charged particle pseudorapidity density at  $\sqrt{s} = 900$  GeV,"* arXiv:0911.5430 [hep-ex].
- [31] G. Aad *et al.* [ATLAS Collaboration], Nature Commun. **2** (2011) 463 [arXiv:1104.0326 [hep-ex]].
- [32] CMS Physics Analysis Summary: "Measurement of the inelastic pp cross section at  $s = 7$  TeV with the CMS detector", 2011/08/27.
- [33] F. Ferro [TOTEM Collaboration], AIP Conf. Proc. **1350** (2011) 172; G. Antchev *et al.* [TOTEM Collaboration], Europhys. Lett. **96** (2011) 21002, **95** (2011) 41001 [arXiv:1110.1385 [hep-ex]].
- [34] C. Amsler *et al.* (Particle Data Group), Physics Letters, **B667** (2008) 1.

- [35] A. B. Kaidalov, L. A. Ponomarev and K. A. Ter-Martirosian, *Yad. Fiz.* **44** (1986) 722 [*Sov. J. Nucl. Phys.* **44** (1986) 468]; A. B. Kaidalov, *Phys. Rept.* **50** (1979) 157; A. B. Kaidalov and K. A. Ter-Martirosyan, *Nucl. Phys. B* **75** (1974) 471 and references therein.
- [36] A. Capella, U. Sukhatme, C-I Tan *et al.* *Phys. Rept.* **236**, 225-329 (1994) and references therein.
- [37] E. Gotsman, E. Levin and U. Maor, ‘*Diffraction Production in a Soft Interaction Model: Mass Distributions,*’ arXiv:1302.4524 [hep-ph].
- [38] F. D. Aaron *et al.* [H1 and ZEUS Collaboration], *JHEP* **1001** (2010) 109 [arXiv:0911.0884 [hep-ex]].
- [39] E. Gotsman, E. Levin and U. Maor, *Phys. Rev. D* **84** (2011) 051502 [arXiv:1103.4509 [hep-ph]].
- [40] V. Khachatryan *et al.* [CMS Collaboration], *JHEP* **1101** (2011) 079 [arXiv:1011.5531 [hep-ex]].